Korean Chem. Eng. Res., 59(1), 138-151 (2021)
https://doi.org/10.9713/kcer.2021.59.1.138
PISSN 0304-128X, EISSN 2233-9558

The Onset and Growth of the Buoyancy-driven Fingering Driven by the Irreversible A+B→C Reaction in a Porous Medium: Reactant Ratio Effect

Min Chan Kim†

Department of Chemical Engineering, Jeju National University, Jeju, 63243, Korea
(Received 12 August 2020; Received in revised from 9 September 2020; Accepted 9 September 2020)

Abstract – The effect of a reactant ratio on the growth of a buoyancy-driven instability in an irreversible A+B→C reaction system is analyzed theoretically and numerically. Taking a non-stoichiometric reactant ratio into account, new linear stability equations are derived without the quasi-steady state assumption (QSSA) and solved analytically. It is found that the main parameters to explain the present system are the Damköhler number, the dimensionless density difference of chemical species and the ratio of reactants. The present initial grow rate analysis without QSSA shows that the system is initially unconditionally stable regardless of the parameter values; however, the previous initial growth rate analysis based on the QSSA predicted the system is unstable if the system is physically unstable. For time evolving cases, the present growth rates obtained from the spectral analysis and pseudo-spectral method support each other, but quite differently from that obtained under the conventional QSSA. Adopting the result of the linear stability analysis as an initial condition, fully nonlinear direct numerical simulations are conducted. Both the linear analysis and the nonlinear simulation show that the reactant ratio plays an important role in the onset and the growth of the instability motion.

Key words: Density driven fingering, Irreversible reaction, Reactant ratio effect, Linear stability analysis, Direct numerical simulation

1. Introduction

Buoyancy-driven instability coupled with chemical reaction plays important roles in mixing in micro-fluidic devices [1], geological CO_2 sequestration [2] and CO_2 capture process [3]. Under this background, Almarcha et al. [4, 5] and Kuster et al. [6] experimentally analyzed the effect of gravity on the stability of reactive interface in a Hele-Shaw cell. In their experiments, they employed acid-base reactions which can be treated as infinitely fast reaction. Later, Lemaigre et al. [7] conducted experimental and numerical studies on the onset of Rayleigh-Taylor and double diffusive instability in reactive systems confined within Hele-Shaw cells. Lemaigre et al. [7] experimentally showed that the reactant ratio plays an important role in the type of instability. Very recently, Cherezov and Cardoso [8] experimentally showed that in a partially miscible system, the reactant ratio is important in the prediction of the onset and the growth of gravitational instabilities. In their experiments, they employed a non-stoichiometric acid-base reaction system [7,8].

Theoretically, Hejazi and Azaiez [9,10] considered the viscosity variation and transverse flow effects on the gravitational instability of a reactive front. However, their linear stability analysis strongly depends on the conventional quasi-steady state approximation (QSSA) in the global (τ, z) domain. Even though the conventional QSSA has been widely used to analyze the stability of the fluid systems [9-15], its validity should be carefully checked. As discussed by Tan and Homsy [11] and Trevelyan et al. [12], the validity of their QSSA is questionable, especially at the early stage of diffusion. Therefore, systematic stability analysis without the QSSA is strongly needed to understand the chemical effect on the buoyancy-driven instability. Under this background, Kim [16] conducted systematic linear stability analysis on the onset and growth of gravitational fingering driven by the stoichiometric irreversible chemical reaction using the QSSA in the (τ, ζ) similarity domain. Also, fully non-linear numerical simulations were conducted. Recently, for a partially miscible system, Loodts et al. [17] analyzed the effect of reactant ratio on the onset and the growth of the gravitational fingering theoretically and numerically. Later, Kim and Wylock [18] reconsidered the same system without the QSSA.

In the present study, for a fully miscible system, we focused on the effect of reactant ratio on the onset and the growth of buoyancy-driven instability. Under the linear stability theory, infinitely fast and infinitely slow reactions were considered analytically without the aid of QSSA. Because the temporal evolution of base field is taken into account, the present analysis is the relaxed the previous QSSA where the base fields are frozen at a certain time. Using the result of the linear stability analysis as an initial condition, direct nonlinear simulations were also conducted. Both the analytical and the numerical analyses give nearly same results regardless of the solution method and the calculation domain adopted in these analyses. Since we derived stability equations without any unphysical assumption and solved them analytically, the present study can be used as a base point to study the

† To whom correspondence should be addressed.
E-mail: mckim@cheju.ac.kr

chemical reaction effects on buoyancy-driven convection.

2. Theoretical Analysis

2-1. Governing equations

The system considered here is a Hele-Shaw cell or a two-dimensional porous medium schematized in Fig. 1. Inside a system, a solution of a reactant A at concentration C_{A0} is placed on top of a solution containing a reactant B at concentration $C_{B0}(=rC_{A0})$. A chemical reaction occurs between the two chemical species A and B, and a product C is produced the following irreversible bimolecular elementary reaction:

$$A + B \rightarrow C. \tag{1}$$

If the density of product C is different from that of either reactant, the flow system can be hydrodynamically unstable and induce density-driven convective motion.

The governing equations are those for the conservation of mass, the conservation of momentum in the form of Darcy's law and the convection-diffusion-reaction mass balance equation,

$$\nabla \cdot \mathbf{U} = 0\,, \tag{2}$$

$$\nabla P = -\frac{\mu}{K}\mathbf{U} + \rho\mathbf{g}\,, \tag{3}$$

$$\frac{\partial C_A}{\partial t} + \mathbf{U}\cdot\nabla C_A = D_A\nabla^2 C_A - k_r C_A C_B, \tag{4}$$

$$\frac{\partial C_B}{\partial t} + \mathbf{U}\cdot\nabla C_B = D_B\nabla^2 C_B - k_r C_A C_B, \tag{5}$$

$$\frac{\partial C_C}{\partial t} + \mathbf{U}\cdot\nabla C_C = D_C\nabla^2 C_C + k_r C_A C_B\,, \tag{6}$$

where $\mathbf{U}$ is the velocity vector, μ the viscosity, K the permeability, P the pressure, C_i the concentration of chemical species $i(=A,B$ or $C)$, D_i the diffusion coefficient chemical species i, and k_r the reaction constant of reaction (1). The solution density is assumed to depend linearly on the concentrations as

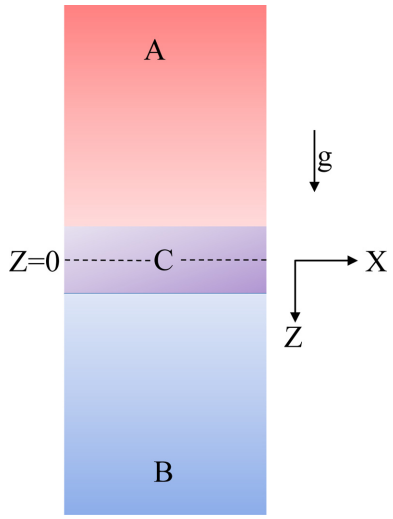

Fig. 1. Schematic diagram of system considered here.

$$\rho = \rho_r\left(1 + \beta_A C_A + \beta_B C_B + \beta_C C_C\right) \tag{7}$$

where ρ_r is the density of the solvent and $\beta_i\left(=\rho_r^{-1}\,\partial\rho/\partial C_i\right)$ the solutal expansion coefficient of species i. It is assumed that the diffusivities of chemical species in the aqueous solution are nearly equal so that $D_A = D_B = D_C = D$ is assumed. This assumption enables us to avoid double-diffusive effects and to attack this system analytically. The above governing equation can be written in dimensionless form:

$$\nabla\cdot\mathbf{u} = 0\,, \tag{8}$$

$$\mathbf{u} = -\nabla p + \mathbf{k}\frac{gK^{3/2}}{D\nu}\bar{\rho}\,, \tag{9}$$

$$\frac{\partial a}{\partial\tau} + \mathbf{u}\cdot\nabla a = \nabla^2 a - Da\times ab\,, \tag{10}$$

$$\frac{\partial b}{\partial\tau} + \mathbf{u}\cdot\nabla b = \nabla^2 b - Da\times ab\,, \tag{11}$$

$$\frac{\partial c}{\partial\tau} + \mathbf{u}\cdot\nabla c = \nabla^2 c + Da\times ab\,, \tag{12}$$

using $\sqrt{K}$, K/D, $D/\sqrt{K}$, $D\mu/K$ used as the length, time, velocity and pressure scale. Here, $\nabla p = \left(\nabla P - \rho_r\mathbf{g}\right)/\left(D\mu/K\right)$, $a = C_A/C_{A0}$, $b=C_B/C_{A0}$, $c=C_C/C_{A0}$, $\bar{\rho} = (\rho-\rho_r)/\rho_r$ and ν is the kinematic viscosity. The Damköhler number, Da, is defined as

$$Da = \frac{k_r C_{A0} K}{D}\,, \tag{13}$$

represents the ratio of hydrodynamic time scale (K/D) to chemical ones $(1/k_r C_{A0})$.

2-2. Base concentration field

From Eqs. (10)-(12), the base-state concentrations $a_0(\tau,z)$, $b_0(\tau,z)$ and $C_0(\tau,z)$ can be obtained by solving the following reaction-diffusion equations:

$$\frac{\partial a_0}{\partial\tau} = \nabla^2 a_0 - Da\times a_0 b_0\,, \tag{14}$$

$$\frac{\partial b_0}{\partial\tau} = \nabla^2 b_0 - Da\times a_0 b_0\,, \tag{15}$$

$$\frac{\partial c_0}{\partial\tau} = \nabla^2 c_0 + Da\times a_0 b_0\,. \tag{16}$$

The exact analytic solution for the above set of base-state equations is not known. However, the above equations can be reduced as

$$\frac{\partial\theta_0}{\partial\tau} = \frac{\partial^2\theta_0}{\partial z^2} \quad\text{and}\quad \frac{\partial\omega_0}{\partial\tau} = \frac{\partial^2\omega_0}{\partial z^2}\,, \tag{17a \& b}$$

where $\theta_0 = (a_0 + c_0)$ and $\omega_0 = (b_0 + c_0)$. The proper initial and boundary conditions are

$$\theta_0(0,z) = 1 - H(z),\ \theta_0(\tau,-\infty) = 1 \text{ and } \theta_0(\tau,\infty) = 0\,. \tag{18a}$$

$$\omega_0(0,z) = rH(z),\ \omega_0(\tau,\infty) = r \text{ and } \omega_0(\tau,-\infty) = 0\,. \tag{18b}$$

The above equations can be easily solved as

$$\theta_0 = \frac{1}{2}\mathrm{erfc}\left(\frac{\zeta}{2}\right) \text{ and } \omega_0 = \frac{r}{2}\mathrm{erfc}\left(-\frac{\zeta}{2}\right), \quad (19a \& b)$$

where $\zeta\left(=z/\sqrt{\tau}\right)$ is a self-similar variable. From the above solution (19), the following relation can be derived:

$$ra_0 + b_0 + (r+1)c_0 = r, \quad (20)$$

Based on this solution, for the infinitely fast reaction or large time asymptote, i.e., $Da\to\infty$ or $Da\tau\to\infty$, where $a_0\left(\tau, z\ge z_f\right)=0$ and $b_0\left(\tau, z\le z_f\right)=0$, the base concentration fields can be obtained as

$$(a_0,b_0,c_0)=\begin{cases}\left(1-\dfrac{(1+r)}{2}\mathrm{erfc}\left(-\dfrac{\zeta}{2}\right),0,\dfrac{r}{2}\mathrm{erfc}\left(-\dfrac{\zeta}{2}\right)\right) & \text{for } \zeta\le\zeta_f\\ \left(0,r-\dfrac{(1+r)}{2}\mathrm{erfc}\left(\dfrac{\zeta}{2}\right),\dfrac{1}{2}\mathrm{erfc}\left(\dfrac{\zeta}{2}\right)\right) & \text{for } \zeta\ge\zeta_f\end{cases}. \quad (21)$$

We can obtain the reaction front position, ξ_f, by solving $\mathrm{erfc}\left(\zeta_f/2\right)=2r/(1+r)$. And, for the infinitely slow reaction case, $Da\to 0$, where $c_0\left(\tau,z\right)=0$, the base concentration fields can be obtained as

$$(a_0,b_0)=\left(\frac{1}{2}\mathrm{erfc}\left(\frac{\zeta}{2}\right),\frac{r}{2}\mathrm{erfc}\left(-\frac{\zeta}{2}\right)\right) \quad (22)$$

Base concentration profiles for the limiting cases of $Da\to\infty$ and $Da\to 0$ are summarized in Fig. 2. As shown, for the limiting case of $Da\to\infty$, the base concentrations of the reactants and the product have singular point at $\xi=\xi_f$. This singularity can be avoided by using θ_0 and ω_0 rather than a_0, b_0 and c_0, because (C_A+C_C), (C_B+C_C) and their fluxes should be continuous.

Based on the density function defined in Eq. (7), the following relations can be derived:

$$\frac{gK^{3/2}}{D\nu}\left(-\frac{\partial\overline{\rho}_0}{\partial z}\right)=\left\{\left(R_A-rR_B\right)\left(-\frac{\partial\theta_0}{\partial z}\right)+\left(R_C-R_B-R_A\right)\left(-\frac{\partial c_0}{\partial z}\right)\right\}, \quad (23)$$

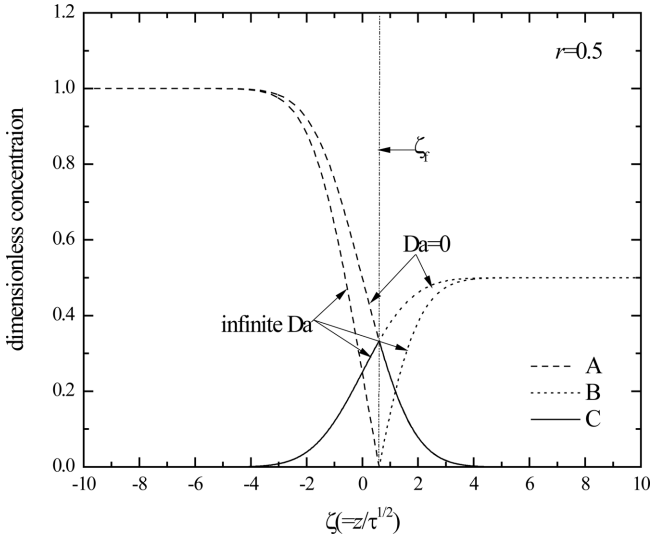

Fig. 2. Base concentration profiles for the infinitely fast and infinitely slow reactions.

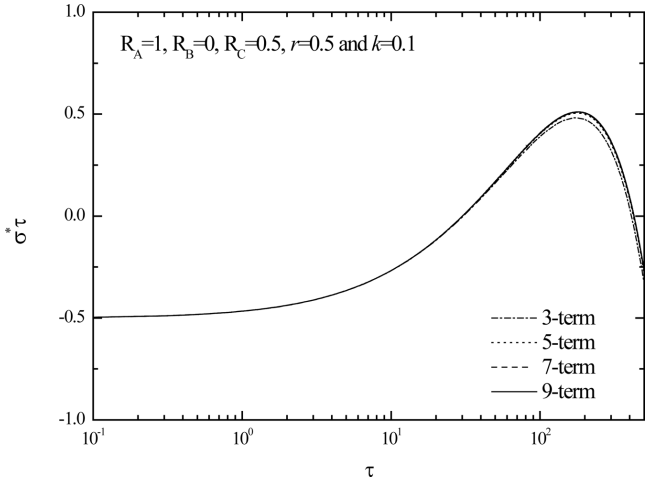

Fig. 3. The growth rates obtained from the various approximations for the specific case of $R_A=1$, $R_B=0$, $R_C=0.5$, $r=0.5$ and $k=0.1$.

where the Rayleigh numbers, R_i's, are defined as

$$R_i=\frac{g\beta_i C_{A0}K^{3/2}}{D\nu}. \quad (24)$$

To discuss the stability characteristics of the system, it is more convenient to express the density gradient as

$$\frac{gK^{3/2}}{D\nu}\left(-\frac{\partial\overline{\rho}_0}{\partial z}\right)=\left\{\left(R_A-\frac{r}{1+r}R_C\right)\left(-\frac{\partial a_0}{\partial z}\right)+\left(\frac{1}{1+r}R_C-R_B\right)\frac{\partial b_0}{\partial z}\right\}, \quad (25)$$

Because at a certain time τ, $(-\partial a_0/\partial z)$ and $(\partial b_0/\partial z)$ are always positive regardless of Da, the system is globally potentially unstable when $R_A > r/(1+r)R_C$ and $(1/r+1)R_C > R_B$. In the opposite case, i.e. $(-\partial\rho_0/\partial z)$ is always negative since $R_A < r/(1+r)R_C$ and $(1/r+1)R_C < R_B$, the system is unconditionally stable. Furthermore, as pointed out by Rongy et al. [19], for a nonzero Da, nonmonotonic density profile is possible (see their Fig. 4) and therefore, locally unstable and stable regions can coexist. Therefore, a careful stability analysis is needed to study the present system. Even

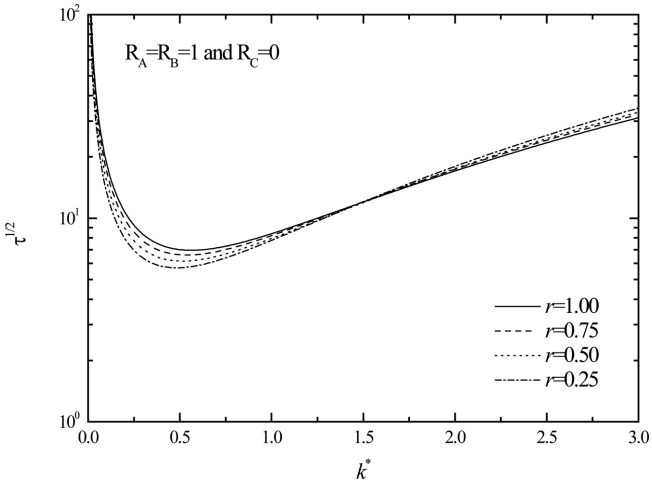

Fig. 4. The effect of the reactant ratio on the neutral stability curves obtained from 9-term approximation for the specific case of $R_A=R_B=1$ and $R_C=0$.

though Trevelyan et al. [20] discussed the effects of the ratio of the reactant concentration, the ratio of the diffusion coefficients, and Rayleigh numbers on density profiles, a linear stability analysis without the QSSA has never been tried.

2-3. Linear stability theory

Under the linear stability theory, the following dimensionless stability equations are obtained by perturbing Eqs. (8)-(12):

$$\nabla^2 w = \frac{gK^{3/2}}{D\nu}\nabla_1^2\bar{\rho}_1 , \tag{26}$$

$$\frac{\partial a_1}{\partial \tau} + w\frac{\partial a_0}{\partial z} = \nabla^2 a_1 - Da\left(a_0 b_1 + a_1 b_0\right) , \tag{27}$$

$$\frac{\partial b_1}{\partial \tau} + w\frac{\partial b_0}{\partial z} = \nabla^2 b_1 - Da\left(a_0 b_1 + a_1 b_0\right) , \tag{28}$$

$$\frac{\partial c_1}{\partial \tau} + w\frac{\partial c_0}{\partial z} = \nabla^2 c_1 + Da\left(a_0 b_1 + a_1 b_0\right) , \tag{29}$$

where the density is decomposed as $\bar{\rho} = \bar{\rho}_0 + \bar{\rho}_1$. And, based on Eq. (7),

$$\bar{\rho}_1 = C_{A0}\left(\beta_A a_1 + \beta_B b_1 + \beta_C c_1\right) , \tag{30}$$

is assumed [20]. Then, Eq. (26) can be reduced as

$$\nabla^2 w = -\nabla_1^2\left(R_A a_1 + R_B b_1 + R_C c_1\right) . \tag{31}$$

The proper boundary conditions for Eqs. (26)-(29) are

$$w \to 0, a_1 \to 0, b_1 \to 0 \text{ and } \to c_1 \to 0 \text{ as } z \to \pm\infty. \tag{32}$$

By rearranging Eqs. (27)-(29), we can obtain the following equations:

$$\frac{\partial \theta_1}{\partial \tau} + w\frac{\partial \theta_0}{\partial z} = \nabla^2\theta_1 \text{ and } \frac{\partial \omega_1}{\partial \tau} + w\frac{\partial \omega_0}{\partial z} = \nabla^2\omega_1 , \tag{33a \& b}$$

where $\theta_1 = \left(a_1 + c_1\right)$, $\omega_1 = b_1 + c_1$, $\frac{\partial \theta_0}{\partial \zeta} = -\frac{1}{\sqrt{\pi}}\exp\left(-\frac{\zeta^2}{4}\right)$ and $\frac{\partial \omega_0}{\partial \zeta} = \frac{r}{\sqrt{\pi}}\exp\left(-\frac{\zeta^2}{4}\right)$. From Eqs. (33a) and (33b), $\omega_1 = -r\theta_1$ can be deduced and therefore, the following relation is hold:

$$ra_1 + b_1 + \left(1+r\right)c_1 = 0 . \tag{34}$$

Based on this relation, for the infinitely fast reaction or large time asymptote, i.e., $Da \to \infty$ or $Da\tau \to \infty$, where $a_1\tau, \xi \ge \xi_f = 0$ and $b_1\tau, \xi \le \xi_f = 0$, the concentration disturbance fields can be obtained as

$$\left(a_1, b_1, c_1\right) = \begin{cases} \left(\left(1+r\right)\theta_1, 0, -r\theta_1\right) & \text{for } \zeta \le \zeta_f \\ \left(0, -\left(1+r\right)\theta_1, \theta_1\right) & \text{for } \zeta \ge \zeta_f \end{cases} , \tag{35}$$

And, for the infinitely slow reaction case, $Da \to 0$, where $c_1(\tau, z) = 0$, the concentration disturbance fields can be obtained as

$$\left(a_1, b_1\right) = \left(\theta_1, -r\theta_1\right) . \tag{36}$$

Since the coefficients of the above equations are independent of x and y, under the normal mode analysis, the Laplacian operator can be expressed as

$$\nabla^2 = \frac{\partial^2}{\partial z^2} + \nabla_1^2 = \frac{\partial^2}{\partial z^2} - k^2 , \tag{37}$$

where $\nabla_1^2 = \partial^2/\partial x^2 + \partial^2/\partial y^2$ and k is the horizontal wavenumber in (x, y) - plane. Finally, with Eqs. (31) and (33) the following stability equations are obtained:

$$\left(\frac{\partial^2}{\partial z^2} - k^2\right)w = -k^2\left(R_A a_1 + R_B b_1 + R_C c_1\right) , \tag{38}$$

$$\frac{\partial \theta_1}{\partial \tau} + w\frac{\partial \theta_0}{\partial z} = \left(\frac{\partial^2}{\partial z^2} - k^2\right)\theta_1 . \tag{39}$$

Ben et al. [21], Riaz et al. [22] and Pritchard [23] mentioned that the disturbances which are localized near the reaction front cannot be accurately captured in (τ, z) - domain, since the dominant operator, $\partial^2/\partial z^2$ does not have localized eigenfunctions that vanish at the infinite boundaries. Following their suggestion, we can reformulate Eqs. (38) and (39) in the similar in (τ, ξ) - domain as

$$\tau\frac{\partial \theta_1}{\partial \tau} - \frac{\zeta}{2}\frac{\partial \theta_1}{\partial \zeta} + \sqrt{\tau}w\frac{\partial \theta_0}{\partial \zeta} = \left(\frac{\partial^2}{\partial \zeta^2} - k^{*2}\right)\theta_1 , \tag{40}$$

$$\left(\frac{\partial^2}{\partial \zeta^2} - k^{*2}\right)w = -k^{*2}\left(R_A a_1 + R_B b_1 + R_C c_1\right) . \tag{41}$$

where $k^* = k\sqrt{\tau}$. For the limiting case of $Da \to \infty$, with the aid of Eqs. (35), Eq. (38) can be reduced as

$$\left(\frac{\partial^2}{\partial \zeta^2} - k^{*2}\right)w^- = -k^{*2}\left(\left(1+r\right)R_A - rR_C\right)\theta_1 \text{ for } \zeta \le \zeta_f , \tag{42a}$$

$$\left(\frac{\partial^2}{\partial \zeta^2} - k^{*2}\right)w^- = -k^{*2}\left\{R_{Phys} - rR_{Chem}\right\}\theta_1 \text{ for } \zeta \le \zeta_f , \tag{42a}$$

$$\left(\frac{\partial^2}{\partial \zeta^2} - k^{*2}\right)w^+ = -k^{*2}\left(-\left(1+r\right)R_B + R_C\right)\theta_1 \text{ for } \zeta \ge \zeta_f , \tag{42b}$$

$$\left(\frac{\partial^2}{\partial \zeta^2} - k^{*2}\right)w^+ = -k^{*2}\left\{R_{Phys} + R_{Chem}\right\}\theta_1 \text{ for } \zeta \ge \zeta_f , \tag{42b}$$

Here, $R_{Phys} = \left(R_A - rR_B\right)$ and $R_{Chem} = \left(R_C - R_A - R_B\right)$. As discussed below Eq. (22), the singularity can be avoided by using Eq. (42) rather than Eq. (41). Also, for another limiting case of $Da \to 0$, Eq. (38) becomes

$$\left(\frac{\partial^2}{\partial \zeta^2} - k^{*2}\right)w = -k^{*2}\left(R_A - rR_B\right)\theta_1 . \tag{43}$$

The proper boundary conditions for Eqs. (40)-(43) are

$$w \to 0 \text{ and } \theta_1 \to 0 \text{ as } \zeta \to \pm\infty . \tag{44}$$

The solutions for the vertical velocity field are given in the Appendix.

2-4. Spectral analysis

Using the generalized Fourier series, the concentration disturbance fields can be expressed as

$$\theta_1 = \sum_{n=0}^{\infty} A_n(\tau)\phi_n(\zeta), \tag{45}$$

where the orthogonal functions $\phi_n(\zeta)$ satisfy the following Sturm-Liouville equation:

$$\mathcal{L}\phi_n = -\lambda_n \phi_n, \tag{46}$$

under the following boundary conditions:

$$\phi_1 \to 0 \text{ as } \zeta \to \pm\infty. \tag{47}$$

where L = (D^2 + ζ / 2D) and $D = d/d\zeta$. The solutions of Eqs. (46) and (47) are

$$\frac{1}{A_n}\frac{dA_n}{d\ln\tau} = \frac{1}{\phi_n}\mathcal{L}\phi_n = -\lambda_n \text{ and } \lambda_n = \frac{n+1}{2}, \text{ for } n = 0,1,2,..., \tag{48a \& b}$$

$$\phi_n(\xi) = (-1)^n \kappa_n H_n\left(\frac{\xi}{2}\right)\exp\left(-\frac{\xi^2}{4}\right), \tag{48c}$$

$$\kappa_n = \left\{\sqrt{\left(n!2^{n+1}\sqrt{\pi}\right)}\right\}^{-1}. \tag{48d}$$

where H_n's are the n-th Hermite polynomials. Since the functions ϕ_n's are orthonormal, for any functions ϕ_n and ϕ_m

$$\langle \phi_n, \phi_m \rangle = \int_{-\infty}^{\infty} \phi_n \phi_m \exp\left(\zeta^2/4\right) d\zeta = \delta_{nm}, \tag{49}$$

where $\exp(\zeta^2/4)$ is the weight function of Eq. (48a). <f, g> is called the inner product of the function f and g.

The solution of Eqs. (42) and (43) can be obtained by using the method of the variation of the parameters as

$$w = \frac{k^*}{2}\left[\exp\left(k^*\zeta\right)\int_{\zeta}^{\infty} R\exp\left(-k^*\xi\right)\theta_1 d\xi + \exp\left(-k^*\zeta\right)\int_{-\infty}^{\zeta} R\exp\left(k^*\xi\right)\theta_1 d\xi\right], \tag{50}$$

where $R = \begin{cases} R_- = R_{Phys} - rR_{Chem} & \zeta \le \zeta_f \\ R_+ = R_{Phys} + R_{Chem} & \zeta \ge \zeta_f \end{cases}$ for $Da \to \infty$ and $R = R_{phys}$ for $Da = 0$. By combining Eq. (45) and (50), the following relation can be derived:

$$\begin{aligned} w &= \frac{k^*}{2}\sum_{n=0}^{\infty} A_n\left[\exp\left(k^*\zeta\right)\int_{\zeta}^{\infty} R\exp\left(-k^*\xi\right)\psi_n(\xi)d\xi \right. \\ &\qquad \left. + \exp\left(-k^*\zeta\right)\int_{-\infty}^{\zeta} R\exp\left(k^*\xi\right)\psi_n(\xi)d\xi\right] \\ &= \sum_{n=0}^{\infty} A_n(\tau)\psi_n\left(k^*,\zeta\right) \end{aligned}. \tag{51}$$

Applying these solutions into Eqs. (38) and (39), and performing orthogonalization process, we obtain the following time-evolving equation:

$$\tau\frac{d\mathbf{a}}{d\tau} = \mathbf{E}\mathbf{a}, \tag{52a}$$

$$\mathbf{a} = \left[A_0, A_1, A_2 \cdots\right]^T, \tag{52b}$$

$$\begin{aligned} [\mathbf{E}]_{ij} &= \int_{-\infty}^{\infty} \exp\left(\frac{\zeta^2}{4}\right)\phi_{j-1}\left(\mathcal{L} - k^{*2}\right)\phi_{i-1}d\zeta + \frac{\sqrt{\tau}}{2\sqrt{\pi}}\int_{-\infty}^{\infty}\phi_{j-1}\psi_{i-1}d\zeta \\ &= -\left(\lambda_{i-1} + k^{*2}\right)\delta_{ij} + \frac{\sqrt{\tau}}{2\sqrt{\pi}}\int_{-\infty}^{\infty}\phi_{j-1}\psi_{i-1}d\xi \end{aligned}. \tag{52c}$$

2-5. Generalized stability theory (GST)

The magnitude of the disturbance can be defined as the norm of θ_1 as

$$\|\theta_1\| = \langle\theta_1, \theta_1\rangle = \left[\int_{-\infty}^{\infty}\theta_1^2\exp\left(\zeta^2/4\right)d\zeta\right]^{1/2}, \tag{53}$$

which involves the inner product of ϕ_1 with itself. It is interesting that the above inner product is corresponding to the inner (scalar) product of a spectral coefficient vector with itself as

$$\|\theta_1\| = \left[\mathbf{a}\cdot\mathbf{a}\right]^{1/2} = \left[\mathbf{a}^T\mathbf{a}\right]^{1/2}, \tag{54}$$

Therefore, the growth rate σ* can be expressed as

$$\begin{aligned} \sigma^* &= \frac{1}{\|\theta_1\|}\frac{d\|\theta_1\|}{d\tau} = \frac{1}{2}\frac{1}{\mathbf{a}^T\mathbf{a}}\left(\frac{d\mathbf{a}^T}{d\tau}\mathbf{a} + \mathbf{a}^T\frac{d\mathbf{a}}{d\tau}\right) \\ &= \frac{1}{2}\frac{1}{\mathbf{a}^T\mathbf{a}}\mathbf{a}^T\left(\mathbf{E}^T + \mathbf{E}\right)\mathbf{a}. \end{aligned} \tag{55}$$

Through the eigen analysis method explained in Kim and Choi [24], it can be shown that

$$\sigma^*\tau = \max\left\{\text{eig}\left(\frac{\mathbf{E} + \mathbf{E}^T}{2}\right)\right\}. \tag{56}$$

Therefore, the growth rate can be determined from its maximum eigenvalue. Since the eigenvalue of the normal matrix is real, the growth rate has real value and, therefore, no oscillatory motion can be expected.

For the specific case of $R_A = 1$, $R_B = 0$, $R_C = 0.5$, $r = 0.5$ and $k = 0.1$, the effect of the number of terms used in the analysis is summarized in Fig. 3. This figure shows that the number of terms has little effect on the growth rate during the initial period and initial growth rate approach $\sigma\tau \to 1/2$ as $\tau \to 0$. Some neutral stability curves obtained by setting $\sigma \to 0$ are summarized in Fig. 4. The linear stability conditions are determined by the minimum point of each curve. Fig. 4 shows that for the specific case of $R_A = R_B = 1$ and $R_C = 0$, the system becomes stable as the ratio of reactants concentration increases.

2-6. Initial value problem approach (IVPA)

One of the important advantages of the spectral expansion is that an initial value problem approach is possible in the (τ, ζ) - domain. The partial differential Eqs. (40) and (41) are reduced into a system

of initial value ordinary differential equations as

$$\tau\frac{dA_n}{d\tau}=-\left(\lambda_n+a^2\tau\right)A_n+\tau^{1/2}\frac{1}{2\sqrt{\pi}}\sum_{m=0}^{\infty}A_m\int_{-\infty}^{\infty}\phi_n\psi_m d\zeta\,,$$

for $n = 0, 1, 2, \ldots\infty$. (57)

For the limiting case of $\tau\to 0$, the above equation can be reduced as

$$\tau\frac{dA_n}{d\tau}=-\lambda_n A_n\,,\ \text{for } n=0,\,1,\,2,\,\ldots\infty\,. \tag{58}$$

Therefore, the growth rate of n-th mode disturbance can be represented as

$$\sigma_n^*\tau=-\lambda_n\,, \tag{59}$$

where $\sigma_n^*=\frac{1}{A_n}\frac{dA_n}{d\tau}$. The above relation means that for the limiting case of $\tau\to 0$, the most unstable mode disturbance is the zeroth one and its growth rate is $\sigma_0\tau = -1/2$. This growth rate, also, can be obtained for the long-wave limit $k\to 0$ and finite time, i.e. $k\sqrt{\tau}\to 0$. From these, the proper initial condition is assumed to be

$$\theta_1=A_0(\tau)\frac{1}{\sqrt{2\sqrt{\pi}}}\exp\left(-\frac{\zeta^2}{4}\right)\ \text{at}\ \tau=\tau_i, \tag{60}$$

where τ_i is chosen as a small value but not 0, to avoid a singularity at $\tau = 0$.

To trace the growth history of the disturbances, from Eqs. (53) and (54) the growth rate is defined as

$$\sigma^*=\frac{1}{2}\frac{1}{\mathbf{a}^T\mathbf{a}}\frac{d\left(\mathbf{a}^T\mathbf{a}\right)}{d\tau}\,. \tag{61}$$

For a specific case, the effects of the initiation time τ_i on the growth rate and maximum θ_1 are given in Fig. 5. As shown, the growth rate defined in Eq. (61) is insensitive to the initiation time τ_i. Here, this initial value problem approach in the (τ,ζ) - domain is called IVPA2.

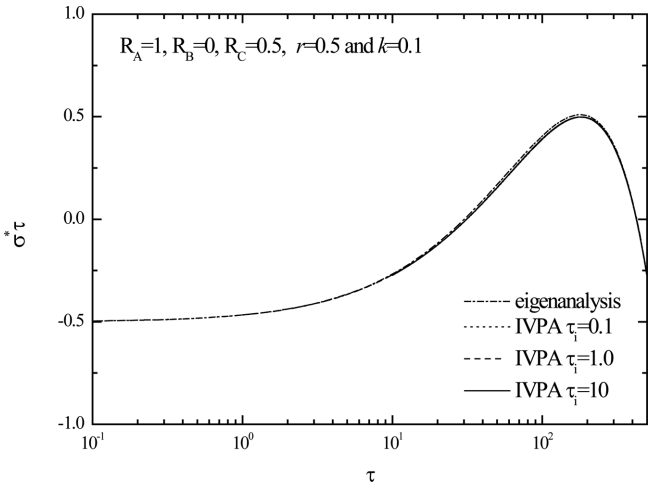

Fig. 5. Comparison of the growth rates obtained from the eigen analysis and IVPA for the specific case of $R_A = 1$ $R_B = 0$ and $R_C = 0.5$, $r = 0.5$ and k = 0.1. The initiation time is not important if $\tau_i \le 10$.

2-7. Quasi-steady state approximations

Conventionally, this kind of problem has been analyzed under the quasi-steady state approximation (QSSA) in the (τ, z) - domain (here, we call it QSSA1) [9-15]. Under the QSSA1, the disturbance quantities are expressed as

$$\left[w(\tau,z),a_1(\tau,z),b_1(\tau,z)\right]=\left[w(z),a_1(z),b_1(z)\right]\exp(\sigma\tau)\,. \tag{62}$$

For the initial state of $\tau = 0$, by applying the above QSSA into Eqs. (26)-(29), the following stability equations can be obtained:

$$\left(\frac{d^2}{dz^2}-k^2-\sigma\right)a_1=Da\times b_1\,, \tag{63a}$$

$$\left(\frac{d^2}{dz^2}-k^2-\sigma-Da\right)b_1=0\,, \tag{64a}$$

$$\left(\frac{d^2}{dz^2}-k^2\right)w=-k^2\left\{\left(R_A-\frac{rR_C}{1+r}\right)a_1+\left(R_B-\frac{R_C}{1+r}\right)b_1\right\}, \tag{65a}$$

for $z < 0$, and

$$\left(\frac{d^2}{dz^2}-k^2-\sigma-rDa\right)a_1=0\,, \tag{63b}$$

$$\left(\frac{d^2}{dz^2}-k^2-\sigma\right)b_1=rDa\times a_1\,, \tag{64b}$$

$$\left(\frac{d^2}{dz^2}-k^2\right)w=-k^2\left\{\left(R_A-\frac{rR_C}{1+r}\right)a_1+\left(R_B-\frac{R_C}{1+r}\right)b_1\right\}, \tag{65c}$$

for $z > 0$, under the following matching conditions:

$$\left[a_1\right]_{0^-}^{0^+}=\left[b_1\right]_{0^-}^{0^+}=\left[w\right]_{0^-}^{0^+}=\left[dw/dz\right]_{0^-}^{0^+}=0\,,\ \left[da_1/dz\right]_{0^-}^{0^+}=-w(0)$$

$$\text{and}\ \left[db_1/dz\right]_{0^-}^{0^+}=rw(0)\,. \tag{66}$$

Following the standard procedure explained in Hejazi and Azaiez [9,10], the above equations have the following solutions:

$$a_1=A^-\exp\left(\gamma_1 z\right)+B^-\exp\left(\gamma_0^- z\right), \tag{67a}$$

$$b_1=B^-\exp\left(\gamma_0^- z\right), \tag{68a}$$

$$w=G^-\exp(kz)-\frac{k^2A^-}{\left(\gamma_1^2-k^2\right)}\left(R_A-\frac{R_C}{2}\right)\exp\left(\gamma_1 z\right)$$
$$-\frac{k^2B^-}{\left(\gamma_0^{-2}-k^2\right)}\left(R_A+R_B-R_C\right)\exp\left(\gamma_0^- z\right)\,, \tag{69a}$$

for $z < 0$, and

$$a_1=A^+\exp\left(-\gamma_0^+ z\right), \tag{67b}$$

$$b_1=A^+\exp\left(-\gamma_0^+ z\right)+B^+\exp\left(-\gamma_1 z\right), \tag{68b}$$

$$w=G^+\exp(-kz)-\frac{k^2A^+}{\left(\gamma_0^{+2}-k^2\right)}\left(R_A+R_B-R_C\right)\exp\left(-\gamma_0^+ z\right)$$
$$-\frac{k^2B^+}{\left(\gamma_1^2-k^2\right)}\left(R_B-\frac{R_C}{1+r}\right)\exp\left(-\gamma_1 z\right)\,, \tag{69b}$$

for $z > 0$, where $\gamma\,\gamma_0^-=\sqrt{k^2+\sigma+Da}$, $\gamma_0^+=\sqrt{k^2+\sigma+rDa}$ and

$\gamma_1 = \sqrt{k^2+\sigma}$. By applying the matching condition (66) on the above solutions, the initial growth rate based on the QSSA1 can be obtained as

$$\gamma_1 = \frac{1}{(\gamma_1+k)}\frac{k}{4}\left\{(1+r)R_A-(1+r)R_B+(1-r)R_C\right\} -(1+r)\frac{k}{4}\left\{\begin{array}{l}\dfrac{1}{\gamma_0^+ +k}-\left(\dfrac{1}{\gamma_0^- +k}+\dfrac{1}{\gamma_0^+ +k}\right)\dfrac{1}{\gamma_0^+ +\gamma_0^-}\\ \left(\gamma_0^+ +\dfrac{r-1}{r+1}\gamma_1\right)\end{array}\right\}R_{Chem}\,. \tag{70}$$

For the instantaneous reaction, $Da\to\infty$, the above relation becomes

$$\gamma_1 = \frac{1}{(\gamma_1+k)}\frac{k}{4}\left\{(1+r)R_A-(1+r)R_B+(1-r)R_C\right\}. \tag{71}$$

For the stoichiometry ratio, $r = 1$, the above relation is reduced as

$$\gamma_1(\gamma_1+k)=\frac{k}{2}(R_A-R_B), \tag{72a}$$

or equivalently as

$$\sigma=\frac{k}{2}\left[(R_A-R_B)-k-\sqrt{k^2+2k(R_A-R_B)}\right], \tag{72b}$$

regardless of *Da*. For the non-reactive case which corresponds to $R_C-R_A-R_B = 0$, the relation can be degenerated as

$$\gamma_1(\gamma_1+k)=\frac{k}{2}R_{Phys}, \tag{73a}$$

or equivalently

$$\sigma=\frac{k}{2}\left[R_{phys}-k-\sqrt{k^2+2kR_{phys}}\right]. \tag{73b}$$

The above relations (73) and (74) imply that the system can be initially unstable for $0<k<R_{Phys}/4$. The maximum growth rate $\sigma_{max} = 5(\sqrt{5}-11)R_{Phys}^2/8$ occurs at the most unstable wavenumber $k_{max} = (\sqrt{5}-2)R_{Phys}/2$. These stability characteristics are identical to Tan and Homsy's [11]. Even though the above QSSA1 has been widely used to analyze the stability of the fluid systems, its validity should be carefully checked. As discussed by Tan and Homsy [11] and Trevelyan et al. [12], the validity of their QSSA1 is questionable especially at the early times. The present analysis without the QSSA suggests that the present system is initially stable. This is the one of the critical differences between the previous studies and the present one.

Using the QSSA in the (τ, ζ) - domain (here we call it QSSA2) [24, 25], the disturbance quantities can be expressed as

$$\left[w(\tau,\zeta),\theta_1(\tau,\zeta)\right]=\left[w(k^*,\zeta),\theta_1(\zeta)\right]\exp(\sigma^*\tau). \tag{74}$$

Substituting the above relation into Eq. (40), the following relation can be derived:

$$\left(D^2+\frac{\zeta}{2}D-k^{*2}-\sigma^*\tau\right)\theta_1=-\frac{\sqrt{\tau}}{2\sqrt{\pi}}\exp\left(-\frac{\zeta^2}{4}\right)w \tag{75}$$

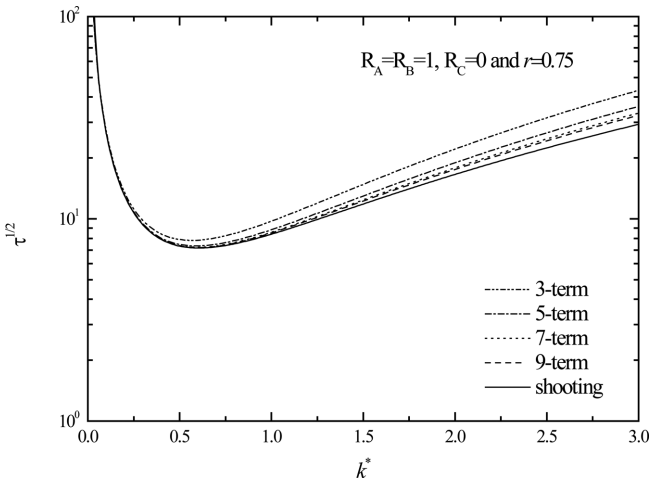

Fig. 6. Neutral stability curves under the QSSA2 for the specific case of $R_A = R_B = 1$, $R_C = 0$ and r = 0.75. Neutral stability curves obtained from the various approximations and the numerical shooting method are compared.

For the limiting case of $Da\to\infty$, Eq. (42) can be reduced as

$$\left(D^2-k^{*2}\right)w^- = -k^{*2}\left(R_{Phys}-rR_{Chem}\right)\theta_1 \quad \text{for} \quad \zeta\le\zeta_f\,, \tag{76a}$$

$$\left(D^2-k^{*2}\right)w^+ = -k^{*2}\left(R_{Phys}+R_{Chem}\right)\theta_1 \quad \text{for} \quad \zeta\ge\zeta_f\,. \tag{76b}$$

And, for another limiting case of $Da\to 0$, Eq. (43) becomes

$$\left(D^2-k^{*2}\right)w = -k^{*2}R_{Phys}\theta_1\,, \tag{77}$$

where $D = d/d\zeta$. The proper boundary conditions for Eqs. (79)-(81) are

$$w\to 0 \text{ and } \theta_1\to 0 \text{ as } \zeta\to\pm\infty\,. \tag{78}$$

Using the similar procedure to obtain Eq. (60), the growth rate can be obtained as

$$\sigma^*\tau = \max\{\mathrm{eig}(\mathbf{E})\}\,. \tag{79}$$

Note that the present QSSA2 is identical with the exact solution for the limiting case of $\mathbf{E} = \mathbf{E}^T$. Also, the above equations can be solved with the well-known shooting method [24]. For the specific case of $R_A = R_B = 1$, $R_C = 0$ and $r = 0.75$, the neutral stability curves based on the Eq. (80) and the numerical shooting solution are compared in Fig. 6. As shown, the critical conditions determined by the minimum points of each curves are relatively insensitive to the number of terms used in Eq. (80).

3. Numerical Simulation

3-1. Stream function-vorticity formulation and Fourier spectral method

Even though the above analyses give useful information on the onset and the growth of the instabilities, more exact solution can be obtained by solving the initial value problem of Eqs. (7)-(11). By

following Tan and Homsy's [26] stream function-vorticity formulation, the following equations can be derived:

$$\nabla^2\psi = -\omega_1 , \tag{80}$$

$$\frac{\partial\theta_1}{\partial\tau} + j = \nabla^2\theta_1 , \tag{81}$$

$$\omega_1 = R_A\left(\frac{\partial a_1}{\partial y}\right) + R_B\left(\frac{\partial b_1}{\partial y}\right) + R_C\left(\frac{\partial c_1}{\partial y}\right). \tag{82}$$

$$j = \left(\frac{\partial\psi}{\partial x}\frac{\partial\theta_0}{\partial z} + \frac{\partial\psi}{\partial x}\frac{\partial\theta_1}{\partial z} - \frac{\partial\psi}{\partial z}\frac{\partial\theta_1}{\partial x}\right), \tag{83}$$

where $\theta(\tau,x,z) = \theta_0(\tau,z)+\theta_1(\tau,x,z)$ is assumed, and $\theta(\tau,z)$ is given in Eq. (19). For infinite *Da* case, the vorticity given in Eq. (86) can be rewritten as

$$\omega_1^+ = -\left(R_{Phys} + R_{Chem}\right)\left(-\frac{\partial\theta_1}{\partial x}\right) \text{ for } z \geq z_f , \tag{84a}$$

$$\omega_1^- = -\left(R_{Phys} - rR_{Chem}\right)\left(-\frac{\partial\theta_1}{\partial x}\right) \text{ for } z \leq z_f . \tag{84b}$$

Also, for nonreactive system whose *Da* = 0, Eq. (86) can be reduced as

$$\omega_1 = -R_{Phys}\left(-\frac{\partial\theta_1}{\partial x}\right). \tag{85}$$

As discussed in section 2.3, for the limiting case of $R_{Chem} = 0$, it should be noted that $\omega_1 = \omega_1 = \omega_1$ and therefore the chemical reaction does no effect on the onset and the growth of the instability motion.

To solve Eqs. (84)-(89), we have employed the Fourier pseudo-spectral numerical scheme described in Tan and Homsy [26]. Based on the above relations, Eqs. (81)-(83) can be expressed in the Fourier space as

$$\left(k_m^2 + k_n^2\right)\hat{\psi}_{m,n} = \hat{\omega}_{m,n} , \tag{86}$$

$$\frac{d\hat{\theta}_{m,n}}{d\tau} + \hat{j}_{m,n} = -\left(k_m^2 + k_n^2\right)\hat{\theta}_{m,n} . \tag{87}$$

The solution of Eq. (93) can be obtained analytically as

$$\hat{\theta}_{m,n}(\tau) = -e^{-\left(k_m^2+k_n^2\right)\tau}\int_{\tau_i}^{\tau} e^{\left(k_m^2+k_n^2\right)\tau'}\,\hat{j}_{m,n}d\tau' + \hat{\theta}_{m,n}(\tau_i) . \tag{88}$$

The time integration of the above solution is done by using a second order Adam-Bashforth predictor-Adam-Moulton corrector scheme, and the physical counterparts of the Fourier components are obtained by the inverse discrete Fourier transform (IDFT) based on fast Fourier transform (FFT) algorithm.

3-2. Linear analysis

Prior to applying the pseudo-spectral method to the nonlinear simulation, its validity should be checked for the linear case. In the linear region, the convective flux given in Eq. (84) can be simplified as

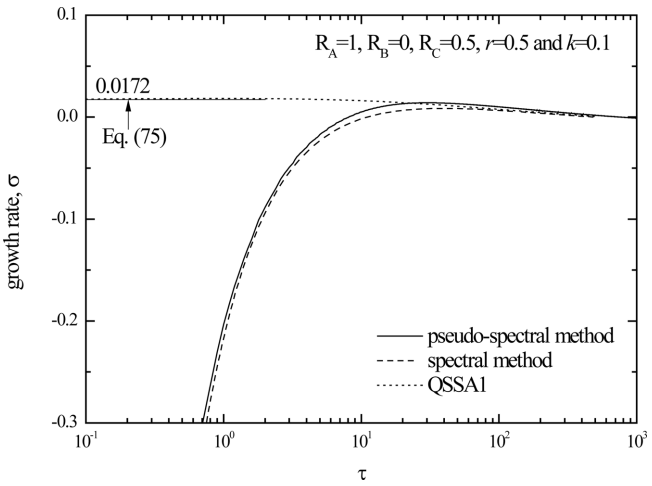

Fig. 7. Comparison of the growth rate obtained from the spectral method and pseudo-spectral one for the case of $R_A = 1$, $R_B = 0$, $R_C = 0.5$, $r = 0.5$ and $k = 0.1$.

$$j = \frac{\partial\psi}{\partial x}\frac{\partial\theta_0}{\partial z} . \tag{89}$$

To start the calculation, proper initial and boundary conditions should be provided. At a excitation time, τ_i, we imposed a small disturbance given in Eq. (64) with a single wavenumber *k* as

$$\theta_1 = \exp\left(-\frac{\zeta_i^2}{4}\right)\sin(kx) , \tag{90a}$$

$$\psi(\tau_i, x, y) = 0 , \tag{90b}$$

here $\zeta_i = z/\sqrt{\tau_i}$, τ_i should be small values. In this linear regime calculation, we set the calculation domain as (l_x, l_y) = (500, λ), here and λ(= 2π / *k*) is the wave length corresponding the wavenumber *k*.

For a specific case of $R_A = 1$, $R_B = 0$, $R_C = 0.5$, $r = 0.5$ and $k = 0.1$, the growth rates calculated from the pseudo-spectral and the spectral methods are compared in Fig. 7. As shown, the conventional QSSA1 predicts that the system has positive growth rate, i.e., the system is unstable, during the initial stage. However, the present study predicts the system has large negative growth rate and, therefore, it is stable during the initial stage. In the QSSA1, the growth rate of the base state is assumed to be very small with respect to that of disturbances. However, this assumption is unphysical because the growth of the base state is very large during the initial stage. This brave assumption caused a difference between the present growth rate and that from the QSSA1 for the small time region, as shown in Fig. 7. This figure also shows that the present growth rate is independent of the solution method and the calculation domain. For the purpose of comparison, the growth rate σ* in the (τ, ξ) - domain is converted into σ in the (τ, z) - one according to the following relation [27]:

$$\sigma\tau = \left(\sigma^*\tau + \frac{1}{4}\right). \tag{91}$$

Recently, Tilton et al. [28] reproduced the above relation.

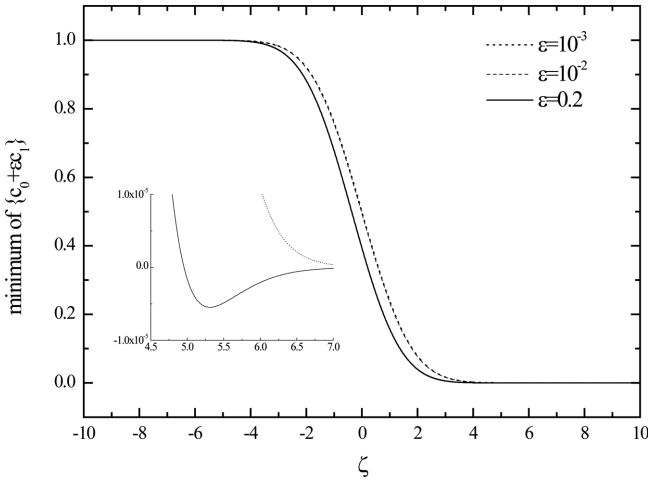

Fig. 8. Effect of the initial disturbance magnitude on the concentration distribution. Insect figure shows that an unphysical negative concentration is possible for $\varepsilon \geq 0.2$.

3-3. Direct numerical simulation (DNS)

In the previous analyses, the wavelength of the disturbances was fixed throughout the simulation. However, the nonlinear phenomena such as wavelength selection mechanism cannot be observed in the single-mode analysis. In this section, the calculation domain is set to [0,2000] × [−1000,1000], and 2048 × 2048 collocation points are used. Unlike the linear theory, the initiation condition is important in the nonlinear analysis. Since the initial growth rate analysis cannot suggest the dominant wavenumber, in the present simulation the following initial condition is employed:

$$\theta_1 = \varepsilon \frac{1}{\sqrt{2\sqrt{\pi}}} \exp\left(-\frac{\zeta_i^2}{4}\right) \mathrm{rand}(x) \quad \text{at} \quad \tau = \tau_i \,, \tag{92}$$

where ε means the initial disturbance level and rand (x) is the pseudo-random number uniformly distributed between −1 and 1. This condition prevents unphysical conditions of $\theta > 1$ or $\theta < 0$, if ε is less than 0.01, as shown in Fig. 8. In the present study, we set $\varepsilon = 0.01$. Recently, Tilton et al. [28] used this kind of initial condition in their DNS study on the onset of convective instability in the carbon dioxide sequestration process. For region of $\tau \sim 0$, the base concentration gradient $\frac{\partial \theta_0}{\partial z}(\sim \delta(z))$ shows non-analytic feature and leads to bad convergence properties. For this reason, at all the non-linear numerical simulations, the disturbance given in Eq. (93) is introduced at $\tau_i = 0.1$.

Here, we are interested in the enhancement of mixing or mass transfer driven by the instability motion, let us consider the mass transfer rate of (A + C). The dimensionless total mass flux at $z = 0$, J, which can be written as the sum of contributions from the base diffusion state, J_0, and the convective motion, J_1:

$$J = J_0 + J_1 \,. \tag{93}$$

The diffusional flux can be computed explicitly from the base concentration profile as

$$J_0 = -\left.\frac{\partial \theta_0}{\partial z}\right|_{z=0} = \frac{1}{\sqrt{4\pi\tau}} \,. \tag{94}$$

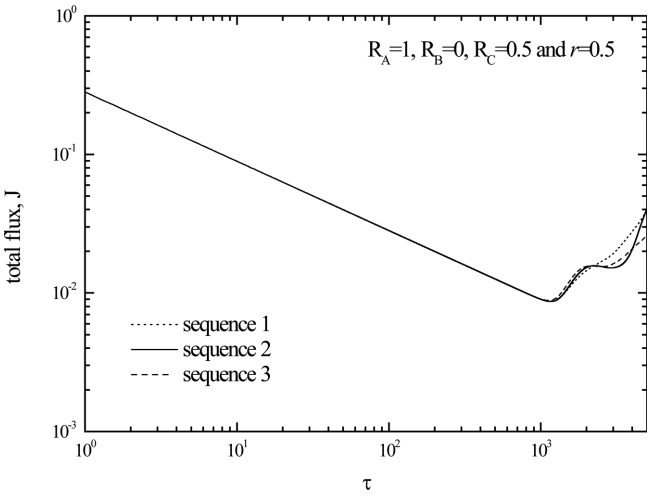

Fig. 9. The effect of random sequence on the total flux for the case of $R_A = 1$, $R_B = 0$, $R_C = 0.5$ and $r = 0.5$. Here the disturbances whose $\varepsilon = 10^{-2}$ are introduced at $\tau_i = 0.1$.

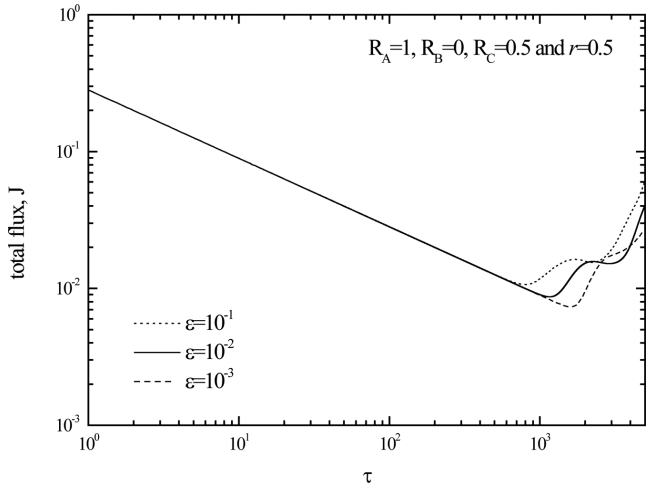

Fig. 10. The effect of initial disturbance level, ε on the total flux for the case of $R_A = 1$, $R_B = 0$, $R_C = 0.5$ and $r = 0.5$. Here the disturbances having various ε are introduced at $\tau_i = 0.1$.

The flux from convective motion is obtained as

$$J_1 = \frac{1}{l_x} \int_0^{l_x} \left\{ -\left.\frac{\partial \theta_1}{\partial z}\right|_{z=0} \right\} dx \,. \tag{95}$$

For the specific case of $R_A = 1$, $R_B = 0$, $R_C = 0.5$ and $r = 0.5$, the effect of the random number sequence on the convective flux is summarized in Fig. 9. As shown, the random number sequence has little effect on the convective flux. Regardless of the random number sequence, the nonlinear effects become sensible after $\tau = 1500$. However, for a real physical system it is difficult to characterize the amplitude and shape of initial disturbances. The effect of the amplitude of the initial disturbance on the convective flux f_1 in Fig. 10, the convective fluxes for three different simulations were given. Regardless of the magnitude of the initial disturbance, during the initial period, diffusion dominates over convection and the disturbances remain in the linear region. It is seen that the

weaker the initial disturbance is, the longer is the time at which the nonlinear terms begin to dominate. Recently, Tilton et al. [28] reported a similar result in their DNS study on the onset of convective instability in the carbon dioxide sequestration process (see their Fig. 10).

4. Results and Discussion

One of the most important stability characteristics is the critical condition for onset of instability. In the present study, the neutral stability curves are obtained by setting $\sigma^* = 0$, and the critical conditions are determined by the minimum point of each curve. However, the conventional QSSA1 cannot be used to obtain the neutral stability curve because it yields that the system is unstable even at $\tau = 0$. For the extreme case of $R_A = R_B = R_C = 1$, the effect of the reactant ratio, r on the neutral stability curve is summarized in Fig. 11. In this case, the system is physically stable, neutral stable and unstable for $r > 1$, $r = 1$ and $r < 1$, respectively. It is interesting that for the case of $r > 1$ the system is physically stable; however, the chemical reaction induces the onset of the fingering instability even in the physically stable system. Usually, chemical species and their physicochemical properties are fixed in real situations, even then we have another parameter r which can control the onset of instability.

For the stoichiometric case ($r = 1$), the neutral stability curves for the cases of (R_A, R_B, R_C) and (R_A, R_B, $2R_A + 2R_B - R_C$) are identical. Rongy et al. [19] and Kim [16] discussed that the flow pattern corresponding(R_A, R_B, R_C) is identical to the flow pattern (R_A, R_B, $2R_A + 2R_B - R_C$) except for the reversal of the flow direction. However, in the nonstoichiometric case ($r \neq 1$), the stability characteristics for both cases are different due to the non-symmetric density profiles. Therefore, we should carefully check the effect of the chemical reaction on the onset of instability.

From Eq. (23), it can be expected that to induce the instability motion, $R_{Phys} > 0$ or $|R_{Chem}| > 0$ should be satisfied. For physically stable systems, i.e., $R_{Phys} < 0$, the chemical effect should overcome

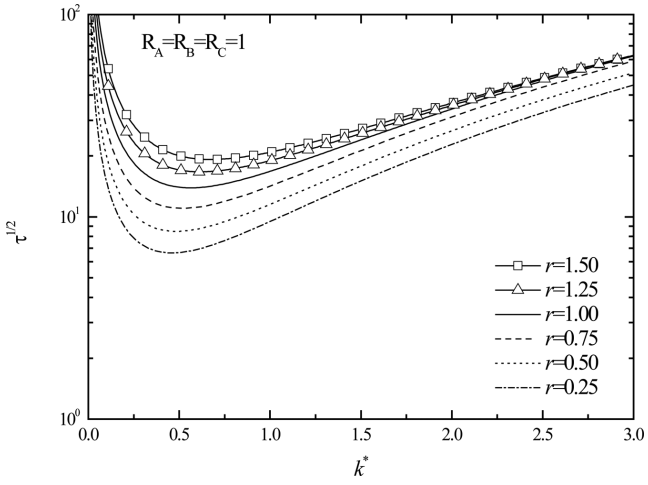

Fig. 11. The effect of the reactant ratio on the neutral stability conditions for the specific case of $R_A = R_B = R_C = 1$.

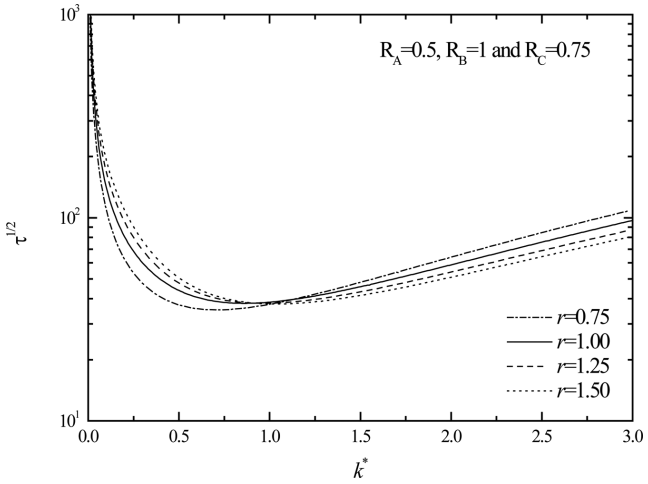

Fig. 12. The effect of the reactant ratio, r on the neutral stability conditions for the physically-stable system of $R_A = 0.5$, $R_B = 1$ and $R_C = 0.75$.

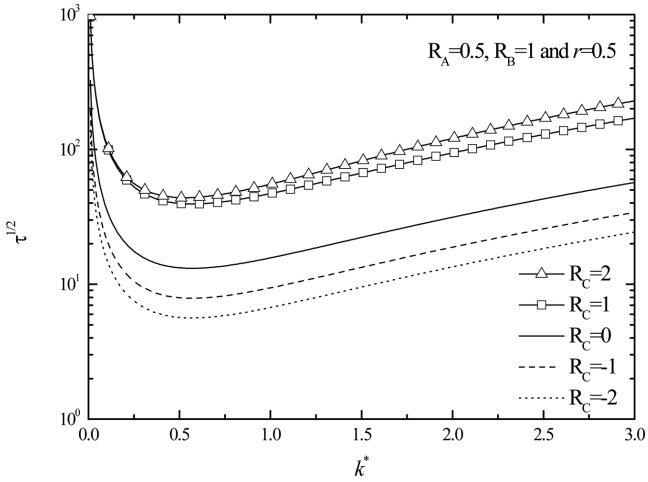

Fig. 13. The effect of the R_C on the neutral stability conditions for the physically-neutral-stable system of $R_A = 0.5$ and $R_B = 1$.

the physically stabilizing effects to insure the onset of convection. The neutral stability curves are summarized for the cases of $R_A = 0.5$ and $R_B = 1$ in Fig. 12. In this case, higher r makes the system physically more stable; however, this stabilizing effect is outbalanced by the destabilizing effect of the chemical reaction. Also, negative R_C promotes the onset of fingering instability. From Eq. (42), it can be expected that for the case of $R_A < (r/(1+r))R_C < rR_B$, the system is unconditionally stable; i.e., σ^* is always negative and therefore for the case of $0 < R_C < (1 + r)$, the neutral stability curves cannot be found in Fig. 12.

In the physically-neutrally-stable case, i.e., $R_{Phys} = 0$, the instability can be induced if $|R_{Chem}| > 0$. The neutral stability curves for the various cases are given in Fig. 13. In the physically stable and neutrally stable systems, i.e., $R_{Phys} \leq 0$, no instability motion can be expected in case of $R_C = (R_A + R_B)$, which corresponds to the non-reactive one and $R_{Chem} = 0$.

In the physically-unstable systems, i.e. $R_{Phys} > 0$, we considered two typical cases $R_C + (R_A + R_B)/2$ and $R_C + (R_A + R_B)$. The density

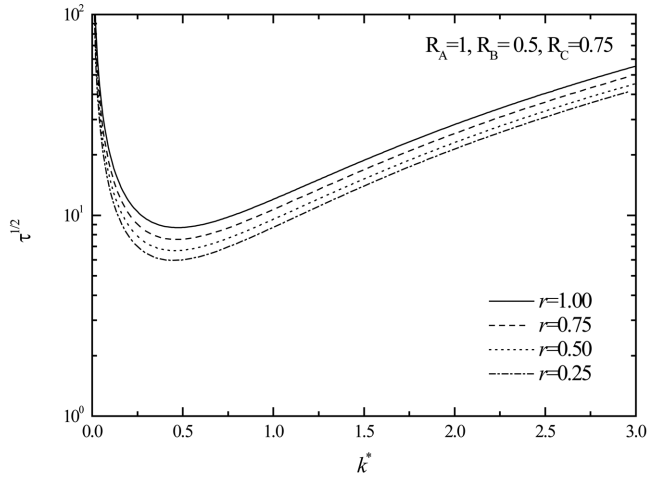

(a) $R_A = 1$, $R_B = 0.5$ and $R_C = 0.75$

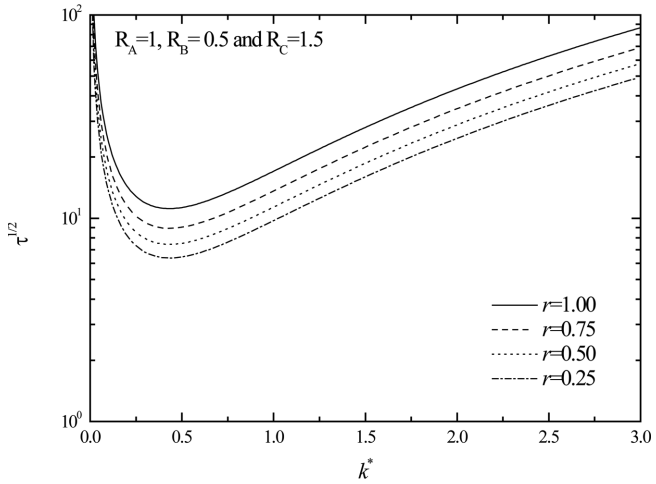

(b) $R_A = 1$, $R_B = 0.5$ and $R_C = 1.5$

Fig. 14. The effect of the reactant ratio, *r* on the neutral stability conditions for the physically-unstable systems. (a) $R_A = 1$, $R_B = 0.5$ and $R_C = 0.75$ and (b) $R_A = 1$, $R_B = 0.5$ and $R_C = 1.5$.

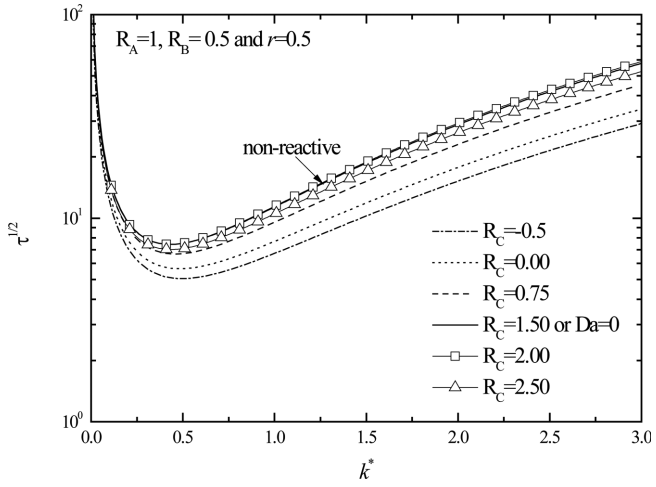

Fig. 15. The effect of the R_C on the neutral stability conditions for the physically-unstable system of $R_A = 1$ and $R_B = 0.5$.

of the product C is the average of the reactants A and B in the former case, and the sum of the reactants A and B in the latter one. The neutral stability curves for the physically-unstable system are summarized in Fig. 14. It is well-known that the non-reactive system ($Da = 0$) is unstable, and the case of $R_{Chem} = 0$ corresponds to the non-reactive one. As shown in Figs. 14(a) and (b), higher R_{Phys}, i.e., lower r, makes the system more unstable. The R_C-effect on the stability conditions is given in Fig. 15. As shown, the non-reactive case corresponds to the upper-bound of the neutral stability curves, that is the chemical reaction makes the system unstable regardless of R_C.

Now, we will consider the growth of disturbance through the nonlinear DNS calculation. For a certain initial disturbance, the effect of the various parameters on the total fluxes is summarized in Figs. 16-20. As shown, the characteristic time τ_m at which the flux starts to deviate from the diffusional one is strongly dependent on R_A, R_B, R_C and r. The effect of the reactant ratio, r on the temporal evolution of the total flux for the physically-stable case of $R_A = 0$, $R_B = 1$ and $R_C = -2$ is summarized in Fig. 16. This figure shows that in the physically-stable system, convective instability can occur for a certain

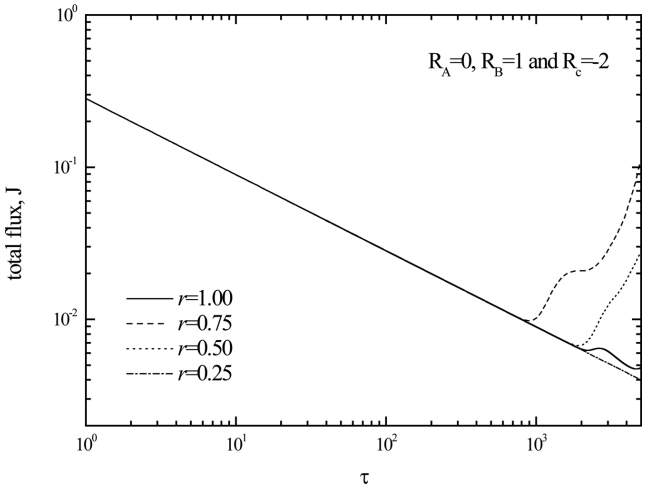

Fig. 16. The effect of the reactant ratio, r on the temporal evolution of the total flux for the physically-stable system of $R_A = 0$, $R_B = 1$ and $R_C = -2$.

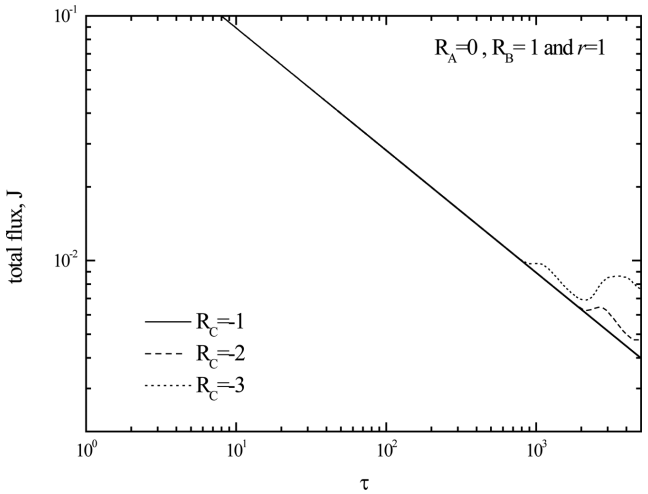

Fig. 17. The effect of R_C on the temporal evolution of the total flux for the physically-stable system of $R_A = 0$, $R_B = 1$ and $r = 1$.

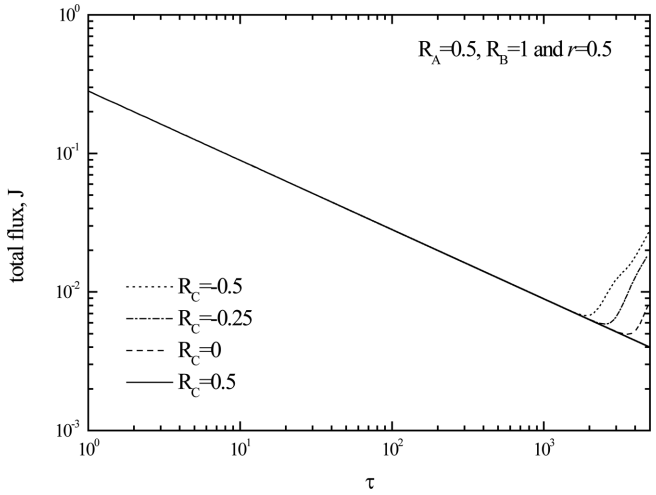

Fig. 18. The effect of the R_C on the temporal evolution of the total flux for the physically-neutrally-stable system of $R_A = 0.5$, $R_B = 1$ and $r = 0.5$.

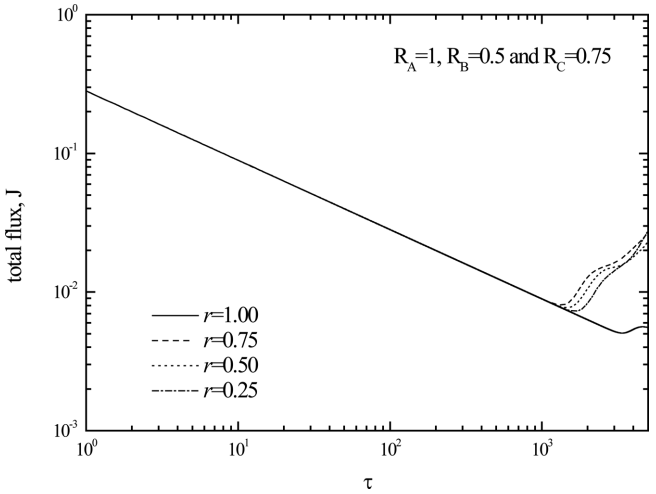

Fig. 19. The effect of the reactant ratio, r on the temporal evolution of the total flux of the physically-unstable system stable system of $R_A = 1$, $R_B = 0.5$ and $R_C = 0.75$.

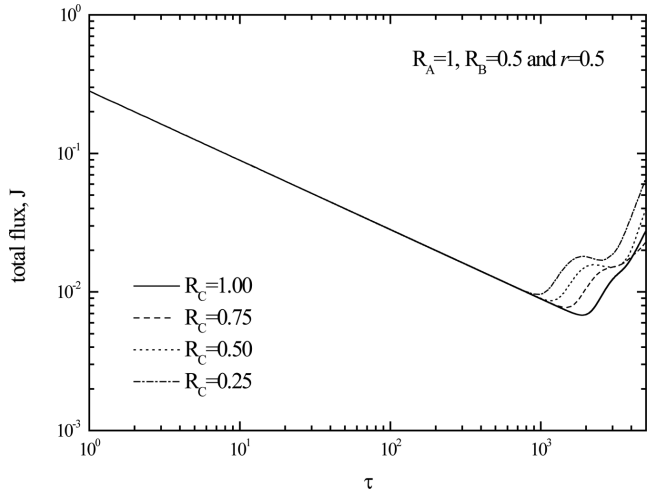

Fig. 20. The effect of the R_C on the temporal evolution of the total flux for the physically-unstable system of $R_A = 1$, $R_B = 0.5$ and $r = 0.50$.

condition and the reactant ratio, r, is an important parameter to analyze the onset of instability. The effect of R_C for the physically-stable case is summarized in Fig. 17. This figure shows that negative R_C accelerates the onset of convection for the physically-stable system. As shown in Fig. 18, for the physically-neutrally-stable system of $R_A = 0.5$, $R_B = 1$ and $r = 0.5$, a similar trend can be found.

For the physically-unstable system stable system of $R_A = 1$, $R_B = 0.5$ and $R_C = 0.75$, the effect of the reactant ratio, r on the onset of nonlinear convection is featured in Fig. 19. This figure shows that the effect of r is not simple and, therefore, we cannot find a general trend. R_C^- effect on the nonlinear convection is also given in Fig. 20. From this figure, like the physically-stable system, the smaller R_C enhanced the convective motion for the physically-unstable system.

5. Conclusions

The effect of reactant ratio on the onset and growth of the buoyancy-driven chemo-convection in a porous medium or a Hele-Shaw cell was studied using linear stability theory and nonlinear direct numerical simulation. By considering the non-stoichiometric reactant ratio, new stability equations were derived without the QSSA and solved analytically and numerically. Through the initial growth rate analysis, it was found that for the limiting case of $\tau \to 0$, the system was unconditionally stable regardless of the density profile. However, the previous analysis based on the QSSA predicted that initially the system is unstable for the physically unstable system, $R_{Phys}(=R_A - rR_B) > 0$. This is the most critical difference between the previous analysis and the present one. For the time evolving case, the growth rate of the disturbance was calculated using the generalized stability theory (GST) and the initial value problem approach (IVPA). Interestingly, the present GST and IVPA show nearly the same result.

It is shown that the chemical reaction can induce the convective motion even in the physically stable or neutrally stable systems, i.e., $R_{Phys} \le 0$. Since the important parameters for the present system are R_{Phys} and R_{Chem} (= $R_C - R_A - R_B$), and R_{Phys} can be controlled by the initial reactant ratio, r, it plays important roles in the stability characteristics. From the present direct numerical simulation (DNS) study, it is found that the convective instability driven by the chemical reaction does deform the reaction front and accelerate the propagation of the reaction front, and the reactant ratio plays a critical role in the onset and the growth of the instability motion.

Acknowledgment

This research was supported by the 2020 scientific promotion program funded by Jeju National University.

References

1. Burghelea, T. L. and Frigaard, L. A., "Unstable Parallel Flows Triggered by a Fast Chemical Reaction," *J. Non-Newt. Fluid*

Mech., **166**, 500-514(2011).
2. Ghoshal, P., Kim, M. C. and Cardoso, S. S. S., "Reactive–convective Dissolution in a Porous Medium: the Storage of Carbon Dioxide in Saline Aquifers," *Phys.Chem.Chem.Phys*., **19**, 644-655 (2017).
3. Wylock, C., Rednikova, A., Colineta, P. and Hauta, B., "Experimental and Numerical Analysis of Buoyancy-induced Instability During CO_2 Absorption in $NaHCO_3$-Na_2CO_3 Aqueous Solutions," *Chem. Eng. Sci*., **157**, 232-246(2017).
4. Almarcha, C., Trevelyan, P. M. J., Grosfils, P. and De Wit, A., "Chemically Driven Hydrodynamic Instabilities," *Phys. Rev. Lett*., **104**, 044501(2010).
5. Almarcha, C., R'Honi, Y., De Decker, Y., Trevelyan, P. M. J., Eckert, K. and De Wit A., "Convective Mixing Induced by Acid-base Reactions," *J. Phys. Chem. B,* **115**, 9739-9744 (2011).
6. Kuster, S., Riolfo, L. A., Zalts, A., El Hasi, C., Almarcha, C., Trevelyan, P. M. J., De Wit, A. and D'Onofrio, A., "Differential Diffusion Effects on Buoyancy-driven Instabilities of Acid–base Fronts: the Case of a Color Indicator," *Phys. Chem. Chem. Phys*., **13**, 17295-17303(2011).
7. Lemaigre, L., Budroni, M. A., Riolfo, L. A., Grosfils, P., De Wit, A., "Asymmetric Rayleigh-Taylor and Double Diffusive Fingers in Reactive Systems," *Phys. Fluids*, **25**, 014103(2013).
8. Cherezov, I. and Cardoso, S. S. S., "Acceleration of Convective Dissolution by Chemical Reaction in a Hele-Shaw Cell, Phys," *Chem. Chem. Phys*., **18**, 23727-23736(2016).
9. Hejazi, S. H. and Azaiez, J., "Stability of Reactive Interfaces in Saturated Porous Media Under Gravity in the Presence of Transverse Flows," *J. Fluid Mech*., **695**, 439-466(2012).
10. Hejazi, S. H. and Azaiez, J., "Nonlinear Simulation of Transverse Flow Interactions with Chemically Driven Convective Mixing in Porous Media," *Water Res. Res*., **49**, 4697-4618(2013).
11. Tan, C. T. and Homsy, G. M., "Stability of Miscible Displacements in Porous Media: Rectilinear Flow," *Phys. Fluids*, **29**, 3549-3556 (1986).
12. Trevelyan, P. M. J., Almarcha, C. and De Wit, A., "Buoyancy-driven Instabilities of Miscible Two-layer Stratifications in Porous Media and Hele-Shaw Cells," *J. Fluid Mech*., **670**, 38-65(2011).
13. Ghesmat, K., Hassanzadeh, H. and Abedi, J., "The Impact of Geochemistry on Convective Mixing in a Gravitationally Unstable Diffusive Boundary Layer in Porous Media: CO_2 Storage in Saline Aquifers," *J. Fluid Mech*., **673**, 480-512(2011).
14. Ghesmat, L., Hassanzadeh, H., Abedi, J. and Chen, Z., "Frontal Stability of Reactive Nanoparticle Transport During in situ Catalytic Upgrading of Heavy Oil," *Fuel*, **107**, 525-538(2013).
15. Loodts, V., Rongy, L. and De Wit, A., "Chemical Control of Dissolution-driven Convection in Partially Miscible Systems: Theoretical Classification," *Phys. Chem. Chem. Phys*., **17**, 29814-29823 (2015).
16. Kim, M. C., "Effect of the Irreversible A+B→C Reaction on the Onset and the Growth of the Buoyancy-driven Instability in a Porous Medium," *Chem. Eng. Sci*., **112**, 56-71(2014).
17. Loodts, V., Thomas, C., Rongy, L. and De Wit, A., "Control of Convective Dissolution by Chemical Reactions: General Classification and Application to CO_2 Dissolution in Reactive Aqueous Solutions," *Phys. Rev. Lett*., **113**, 114501(2014).
18. Kim, M. C. and Wylock, C., "Linear and Nonlinear Analyses of the Effect of Chemical Reaction on the Onset of Buoyancy-driven Instability in a CO_2 Absorption Process in a Porous Medium or Hele-Shaw Cell," *Can. J. Chem. Eng*., **95**, 589-604(2017).
19. Rongy, L., Trevelyan, P. M. J. and De Wit, A., "Influence of Buoyancy-driven Convection on the Dynamics of A+B→C Reaction Fronts in Horizontal Solution Layer," *Chem. Eng. Sci*., **65**, 2382-2391(2010).
20. Trevelyan, P. M. J., Almarcha, C. and De Wit, A., "Buoyancy-driven Instabilities Around Miscible A+B→C Reaction Fronts: A General Classification," *Phys. Rev. E*, **91**, 023001(2015).
21. Ben, Y., Demekhin, E. A. and Chang, H. C., "A Spectral Theory for Small-amplitude Miscible Fingering," *Phys. Fluids*, **14**, 999-1010(2002).
22. Riaz, A., Hesse, M., Tchelepi, H. A. and Orr Jr., F. M., "Onset of Convection in a Gravitationally Unstable Diffusive Boundary Layer in Porous Media," *J. Fluid Mech*., **548**, 87-111(2006).
23. Pritchard, D., "The Linear Stability of Double-diffusive Miscible Rectilinear Displacements in a Hele-Shaw Cell," *Eur. J. Mech. (B/Fluids)*, **28**, 564-577(2009).
24. Kim, M. C. and Choi, C. K., "Some Theoretical Aspects on the Onset of Buoyancy-driven Convection in a Fluid-saturated Porous Medium Heated Impulsively From Below," *Korean J. Chem. Eng*., **32**, 2400-2405(2015).
25. Kim, M. C., "Magnetic Field Effect on the Onset of Soret-driven Convection of a Nanofluid Confined Within a Hele-Shaw Cell," *Korean J. Chem. Eng*., **34**, 189-198(2017).
26. Tan, C. T. and Homsy, G. M., "Simulation of Non-linear Viscous Fingering in Miscible Displacement," *Phys. Fluids*, **31**, 1330-1338 (1988).
27. Kim, M. C. and Choi, C. K., "The Stability of Miscible Displacement in Porous Media: Nonmonotonic Viscosity Profile," *Phys. Fluids*, **23**, 084105(2011).
28. Tilton, N., Daniel, D. and Riaz, A., "The Initial Transient Period of Gravitationally Unstable Diffusive Boundary Layers Developing in Porous Media," *Phys. Fluids*, **25**, 092107(2013).

Appendix

For the limiting case of $Da\to\infty$, ψ_n given Eq. (51) is the solution of the following equations:

$$\left(\frac{\partial^2}{\partial\zeta^2}-k^{*2}\right)\psi_n^- = -k^{*2}\left((1+r)R_A - rR_C\right)\phi_n \quad \text{for } \zeta\le\zeta_f\,, \tag{A1a}$$

$$\left(\frac{\partial^2}{\partial\zeta^2}-k^{*2}\right)\psi_n^+ = -k^{*2}\left(-(1+r)R_B + R_C\right)\phi_n \quad \text{for } \zeta\ge\zeta_f\,. \tag{A1b}$$

By solving the above equation, the following recurrence relations can be obtained:

$$\psi_n^-(k^*,\zeta) = 4k^{*2}\left\{\psi_{n-2}^-(k^*,\zeta) + \left(R_{Phys} - rR_{Chem}\right)\phi_{n-2}(\zeta)\right\} + k^*(1+r)R_{Chem}\exp\left\{k^*(\zeta-\zeta_f)\right\}\left\{\phi_{n-1}(\zeta_f) + 2k^*\phi_{n-2}(\zeta_f)\right\}, \tag{A2a}$$

with

$$\psi_0^-(k^*,\zeta) = -\frac{k^*}{2}\sqrt{\pi}\exp\left(k^{*2}\right)\begin{bmatrix}\left(R_{Phys} - rR_{Chem}\right)\begin{Bmatrix}\exp\left(k^*\zeta\right)\operatorname{erfc}\left(\frac{\zeta}{2}+k^*\right)\\ +\exp\left(-k^*\zeta\right)\operatorname{erfc}\left(-\frac{\zeta}{2}+k^*\right)\end{Bmatrix}\\ +(1+r)R_{Chem}\exp\left(k^*\zeta\right)\operatorname{erfc}\left(\frac{\zeta_f}{2}+k^*\right)\end{bmatrix}, \tag{A2b}$$

$$\psi_1^-(k^*,\zeta) = -k^*\exp\left(k^{*2}\right)\begin{bmatrix}\left(R_{Phys} - rR_{Chem}\right)k^*\sqrt{\pi}\begin{Bmatrix}\exp\left(k^*\zeta\right)\operatorname{erfc}\left(\frac{\zeta}{2}+k^*\right)\\ -\exp\left(-k^*\zeta\right)\operatorname{erfc}\left(-\frac{\zeta}{2}+k^*\right)\end{Bmatrix}\\ -(1+r)R_{Chem}\exp\left(k^*\zeta\right)\begin{Bmatrix}\exp\left(-\left(\frac{\zeta_f}{2}+k^*\right)^2\right)\\ -k^*\sqrt{\pi}\operatorname{erfc}\left(\frac{\zeta_f}{2}+k^*\right)\end{Bmatrix}\end{bmatrix} \tag{A2c}$$

for $\zeta\le\zeta_f$, and

$$\psi_n^+(k^*,\zeta) = 4k^{*2}\left\{\psi_{n-2}^+(k^*,\zeta) + \left(R_{Phys} + R_{Chem}\right)\phi_{n-2}(\zeta)\right\} + k^*(1+r)R_{Chem}\exp\left\{-k^*(\zeta-\zeta_f)\right\}\left\{\phi_{n-1}(\zeta_f) - 2k^*\phi_{n-2}(\zeta_f)\right\}, \tag{A2d}$$

with

$$\psi_0^+(k^*,\zeta) = -\frac{k^*}{2}\sqrt{\pi}\exp\left(k^{*2}\right)\begin{bmatrix}\left(R_{Phys} + R_{Chem}\right)\begin{Bmatrix}\exp\left(k^*\zeta\right)\operatorname{erfc}\left(\frac{\zeta}{2}+k^*\right)\\ +\exp\left(-k^*\zeta\right)\operatorname{erfc}\left(-\frac{\zeta}{2}+k^*\right)\end{Bmatrix}\\ -(1+r)R_{Chem}\exp\left(-k^*\zeta\right)\operatorname{erfc}\left(-\frac{\zeta_f}{2}+k^*\right)\end{bmatrix}, \tag{A2e}$$

$$\psi_1^+(k^*,\zeta) = -k^*\exp\left(k^{*2}\right)\begin{bmatrix}\left(R_{Phys} + R_{Chem}\right)k^*\sqrt{\pi}\begin{Bmatrix}\exp\left(k^*\zeta\right)\operatorname{erfc}\left(\frac{\zeta}{2}+k^*\right)\\ -\exp\left(-k^*\zeta\right)\operatorname{erfc}\left(-\frac{\zeta}{2}+k^*\right)\end{Bmatrix}\\ -(1+r)R_{Chem}\exp\left(-k^*\zeta\right)\begin{Bmatrix}\exp\left(-\left(-\frac{\zeta_f}{2}+k^*\right)^2\right)\\ -k^*\sqrt{\pi}\operatorname{erfc}\left(-\frac{\zeta_f}{2}+k^*\right)\end{Bmatrix}\end{bmatrix}, \tag{A2f}$$

for $\zeta\ge\zeta_f$.

For another limiting case of $Da\to 0$, ψ_n can be obtained as

$$\psi_n = 4k^{*2}\left(\psi_{n-2} + R_{Phys}\phi_{n-2}\right),\ n = 2,\ 3,\ 4..., \tag{A3a}$$

with

$$\psi_0 = -R_{Phys}\frac{k^*}{2}\sqrt{\pi}\exp\left(k^{*2}\right)\left\{\exp\left(k^*\zeta\right)\operatorname{erfc}\left(\frac{\zeta}{2}+k^*\right) + \exp\left(-k^*\zeta\right)\operatorname{erfc}\left(-\frac{\zeta}{2}+k^*\right)\right\}, \tag{A3b}$$

$$\psi_1 = -R_{Phys}k^{*2}\sqrt{\pi}\exp\left(k^{*2}\right)\left\{\exp\left(k^*\zeta\right)\operatorname{erfc}\left(\frac{\zeta}{2}+k^*\right) - \exp\left(-k^*\zeta\right)\operatorname{erfc}\left(-\frac{\zeta}{2}+k^*\right)\right\}. \tag{A3c}$$

For the extreme case of $R_{Chem} = (=R_C - R_A - R_B) = 0$, it should be noted that $\psi_n = \psi_n^- = \psi_n^+$ and therefore the chemical reaction does no effect on the onset of convection, as discussed below Eq. (24).